

## ESTIMATION OF DRAG BEHAVIOUR IN TURBULENT FLOW OVER DISCRETE ROUGH SURFACES

**Guo-Zhen Ma**

Department of Engineering Mechanics  
Taiyuan University of Technology  
Taiyuan 030024, China  
Email: maguozhen@tyut.edu.cn

**Hyung Jin Sung**

Department of Mechanical Engineering  
KAIST  
Daejeon 34141, Republic of Korea  
Email: hjsung@kaist.ac.kr

**Chun-Xiao Xu**

Department of Engineering Mechanics  
Tsinghua University  
Beijing 100084, China  
Email: xucx@tsinghua.edu.cn

**Wei-Xi Huang**

Department of Engineering Mechanics  
Tsinghua University  
Beijing 100084, China  
Email: hwx@tsinghua.edu.cn

### ABSTRACT

Direct numerical simulations (DNSs) with body-fitted grids are performed for a turbulent open-channel flow over rough walls composed of discrete and randomly distributed roughness elements at a friction Reynolds number 540. Two groups of rough-wall cases are employed to assess the scaling formula by systematically varying the coverage and the roughness height. The results show that the mean streamwise velocity and stress profiles are highly dependent on both the area coverage and the roughness height. The roughness function and the peak intensities of streamwise dispersive stresses increase with an increase in the coverage or the roughness height, whereas the peak intensities of the streamwise turbulent Reynolds stresses change oppositely. A linear fitting approach is then applied, which successfully scales the relationship between the roughness function and the area coverage as well as the roughness height, and is further extended as a coupling scale of the height and steepness across the entire rough surface. In the future, we will further investigate the effects of more roughness parameters for this type of rough surfaces, in order to obtain a more comprehensive scaling behaviour.

### INTRODUCTION

Rough-wall turbulence has been studied extensively for nearly a century, dating back to the pioneering rough pipe experiments by Nikuradse in 1933. The existence of roughness leads to an increase in wall friction, causing numerous detrimental effects. However, predicting the rough surface resistance remains an unsolved scientific problem. The diversity of physical parameters associated with roughness elements, including different configurations and arrangements, introduces rich variations into the flow field, and makes the resistance prediction more challenging.

Nikuradse (1933) defined the friction coefficient by measuring the pressure drop inside a rough pipe and plotted the Nikuradse curve for various Reynolds numbers and sand grain roughness heights. Subsequently, numerous research efforts have since been focused on the scaling properties of this curve, with the most representative work being that of Tao (2009), who scaled the whole range of Reynolds numbers, including the transitions from laminar to turbulent flows, onto a single curve by a composite scaling variable. Over the past

decade, scaling work related to physical quantities closely associated with wall friction, such as the roughness function and the equivalent sand grain height, has become a hot research topic for various types of rough surfaces (Chung *et al.*, 2021). The scaling forms have also gradually evolved from single roughness parameter to multi-parameter coupling (Thakkar *et al.*, 2017).

In this study, we primarily investigate the impact on wall friction in randomly scattered rough surfaces by increasing the coverage and the roughness height. In fact, discrete rough surfaces can usually be observed in many practical natural and engineering applications, such as rivets on aircraft, biofouling on ships, and atmospheric surface layer over urban buildings or forest. The rest of the paper is organized as follows. Section 2 describes the governing equations and the numerical set-up; Section 3 presents our results for the turbulence statistics and scaling behaviour; our summary and conclusion are provided in Section 4.

### NUMERICAL SIMULATION

The problem under consideration is a fully developed three-dimensional open-channel turbulent flow over rough walls, which consists of discrete and randomly distributed roughness elements according to

$$\eta_d(x, z) = k \left( 1 + \cos \frac{\pi r(x, z)}{R_0} \right),$$
$$(x - x_0)^2 + (z - z_0)^2 \leq R_0^2,$$

(1)

where  $\eta_d$  is the rough surface elevation,  $r$  is the distance from point  $(x_0, z_0)$ ,  $k$  and  $R_0$  denote the central depth and radius of the roughness elements, respectively. Figure 1 illustrates a schematic diagram of the channel, and a right-handed cartesian frame fixed in the physical space is employed, with  $x$ ,  $y$  and  $z$  denoting the streamwise, vertical and spanwise coordinates, respectively.

The governing equations for the turbulent flow are the dimensionless incompressible Navier-Stokes and continuity equations:

$$\frac{\partial \mathbf{u}}{\partial t} + \mathbf{u} \cdot \nabla \mathbf{u} = -\nabla p + \frac{1}{Re_b} \nabla^2 \mathbf{u}, \quad (2)$$

$$\nabla \cdot \mathbf{u} = 0, \quad (3)$$

where  $\mathbf{u} = (u, v, w)$  are the velocity components and  $Re_b$  is the bulk Reynolds number. The flow is driven by a mean pressure gradient that is dynamically adjusted to maintain a strictly constant flow rate over time. The coordinate transformation is adopted to transform the irregular physical domain into a rectangular computational domain based on the boundary-fitted system. Further details of the numerical method can be found in Ge *et al.* (2010). In the open-channel flow, a free-slip condition is applied at the top boundary and a no-slip condition is applied at the bottom boundary. Periodic boundary conditions are applied in the  $x$  and  $z$  directions.

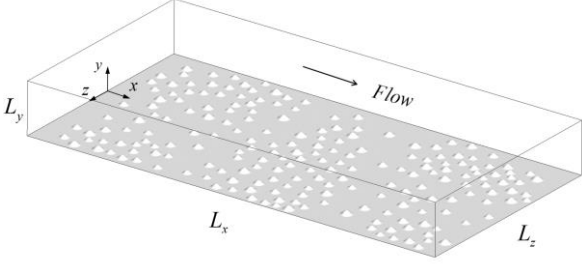


Figure 1. Schematic of the turbulent open-channel flow over a random rough surface.

In the previous study (Ma *et al.*, 2023), we have verified that the aggregated rough surface and dispersed rough surface yield minor discrepancies in wall resistance, when using the same set of roughness elements. Therefore, we only consider two groups of rough-wall cases with randomly distributed roughness elements: (i) the coverage  $\lambda_p$  is varied while the mean roughness height  $\bar{k}_r^+$  is kept constant; (ii) the roughness height  $\bar{k}_r^+$  is varied while the coverage  $\lambda_p$  is kept constant. A summary of the flow and roughness parameters is listed in Table 1, where  $\bar{k}^+$  and  $S$  refer to the height and steepness (Napoli *et al.*, 2008) across the entire rough surface. In all the simulations, the friction Reynolds number is approximately 540. The size of the computational domain is  $4\pi\delta \times \delta \times 2\pi\delta$ , and the corresponding grid number is  $576 \times 192 \times 576$ . The mesh is uniformly spaced in the streamwise and spanwise directions, and stretched in the wall-normal direction according to a cosine distribution. The grid resolution needs to meet the DNS requirements and ensure the smooth recognition of the roughness elements.

Table 1. Flow and roughness parameters.

Case	$Re_b$	$\bar{k}_r^+$	$\lambda_p$ %	$\bar{k}^+$	$S$	$\Delta U^+$
Smooth	9800	--	--	--	--	0
P04	8600	32.4	4.78	1.55	0.054	2.348
P08	8300	33.0	8.93	2.95	0.089	2.812
P16	7800	33.0	16.4	5.42	0.122	3.624
P20	7600	34.1	19.5	6.65	0.191	4.037
P23	7350	33.0	23.4	7.72	0.232	4.585
P26	7200	33.0	26.3	8.68	0.259	4.867
P32	7000	33.0	32.8	10.82	0.328	5.274
H20	9000	20.6	19.0	3.91	0.1	1.519
H25	8600	24.8	19.0	4.72	0.122	2.133

H30	8100	30.2	19.0	5.74	0.151	3.134
H34	7700	33.6	19.0	6.38	0.191	3.686
H39	7400	38.9	19.0	7.39	0.196	4.442

## RESULTS

The effect of roughness elements on the mean velocity profile has been widely studied due to its importance in practical applications. Figure 2 shows the mean streamwise velocity profiles and velocity defects in semi-logarithmic coordinates, where  $\bar{y}$  represents the mean vertical distance from the wall in the boundary-fitted curvilinear coordinate system. Compared to the smooth-wall case, the increase in wall resistance caused by the surface roughness is manifested as a downward shift in the streamwise mean velocity profile in the logarithmic region, known as the Hama roughness function  $\Delta U^+$ . For all rough-wall cases, these mean velocity profiles satisfy the logarithmic-law distribution beyond a certain position as shown in figures 2(a, c). We use the mean offsets in the range  $\bar{y}^+ = 100 \sim 200$  to calculate the roughness function  $\Delta U^+$ , as listed in Table 1. It can be seen that for two group of rough-wall cases,  $\Delta U^+$  both increases as the area coverage and roughness height increase. Both of these results can be interpreted in terms of the average height or steepness of the entire rough surface for discrete roughness elements. Therefore, the current trend is consistent with the variations of the roughness function with respect to roughness height and steepness in previously studied sinusoidal rough-wall turbulence (Ma *et al.*, 2020). By plotting the velocity defect in figures 2(b, d), we observe that the profiles for all rough-wall cases are self-similar in the outer layer. This indicates that the hypothesis of outer-layer similarity holds for the first-order turbulence statistics no matter how the roughness parameters vary.

In order to better represent the relationship among the roughness function, and the area coverage and roughness height, we refer to previously published work (Ma *et al.*, 2020) and employ a linear fitting method to obtain scaling formulas for both the roughness function and the area coverage occupied by roughness, as well as for the roughness height. As depicted in figure 3(a),  $\Delta U^+$  as a function is plotted against  $\lambda_p$  and  $\bar{k}_r^+$ , respectively. All the data collapse onto a single line, i.e.

$$\Delta U^+ = 0.11 \cdot \lambda_p + 1.87, \quad (4)$$

$$\Delta U^+ = 0.16 \cdot \bar{k}_r^+ - 1.7. \quad (5)$$

The goodness-of-fit is close to 0.98 and 0.99 for the above fitting function equations, respectively. In the case with largest  $\lambda_p$ , the roughness function  $\Delta U^+$  is slightly lower than the predicted value. This is primarily due to the increasing number of roughness elements, causing the sheltering effect of upstream roughness elements to become more pronounced. As a result,  $\Delta U^+$  exhibits slow growth and no longer adheres to a linear increasing relationship. According to MacDonald *et al.* (2016),  $\Delta U^+$  begins to decrease when the area coverage is larger than a certain value. However, the current coverage parameter has not yet reached this category. Furthermore, the influence of both the area coverage and roughness height on drag can be recombined as

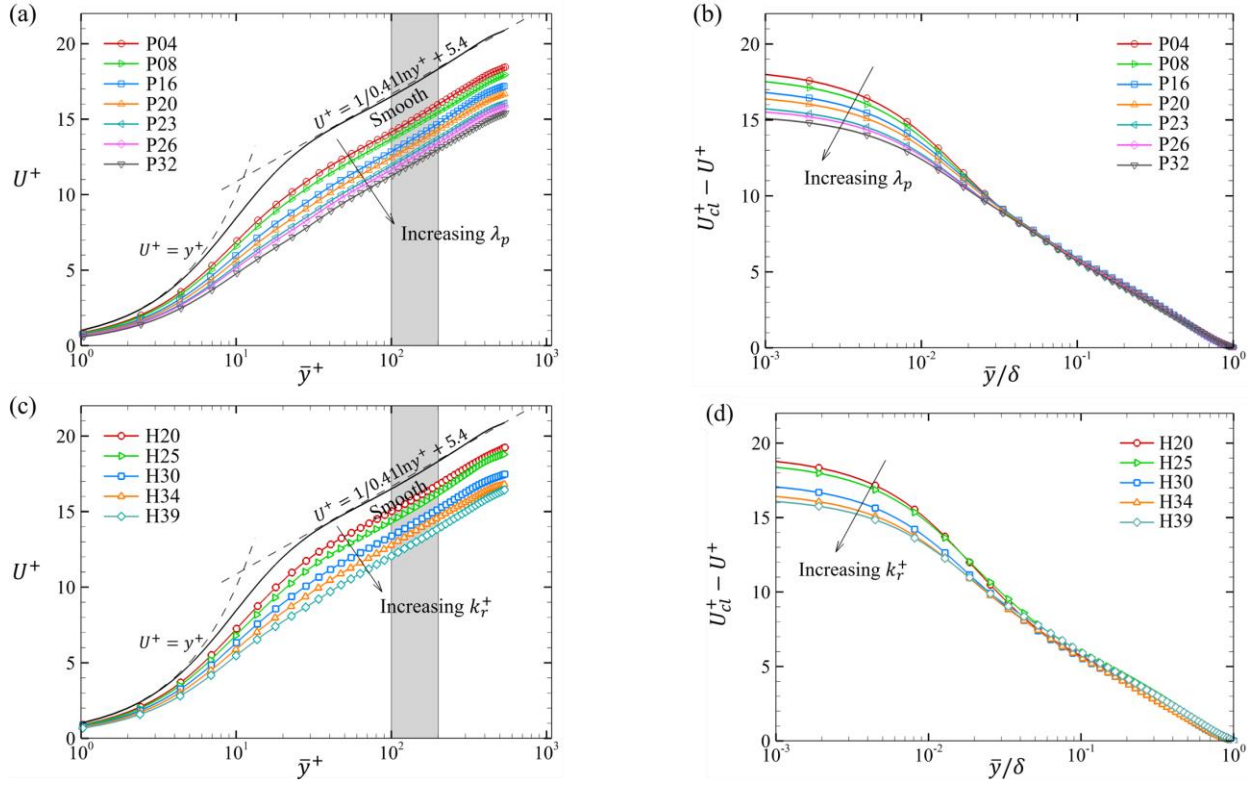


Figure 2. Profiles of (a, c) the mean streamwise velocity plotted against  $\bar{y}^+$  and (b, d) the velocity defects plotted against  $\bar{y}/\delta$  for two groups of rough-wall cases, respectively.

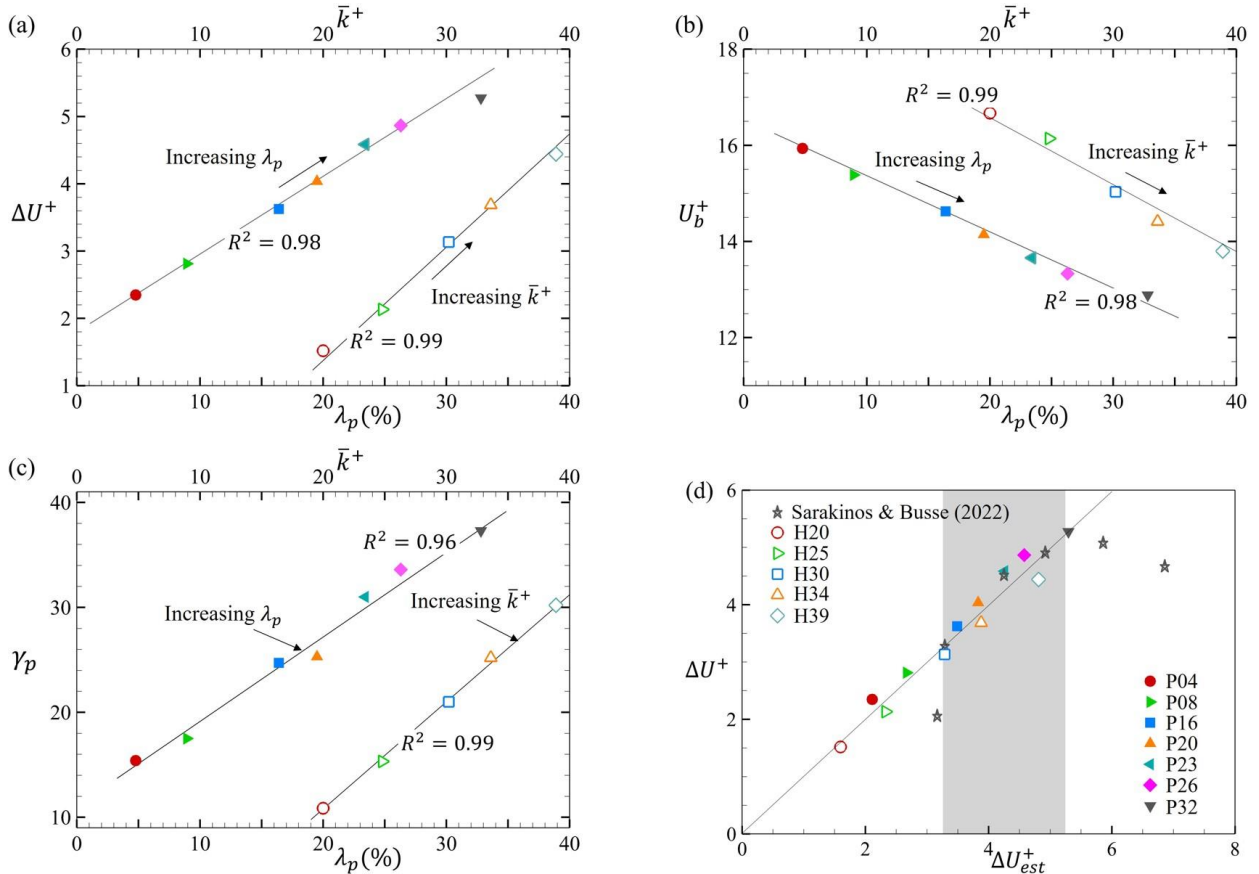


Figure 3. Plots of (a) the roughness function, (b) the viscous-scaled bulk velocity and (c) the ratio of the pressure drag to the total drag force, as a function of the roughness coverage and height, respectively. (d) the actual roughness function versus the predicted roughness function according to Eq. (6).

follows,

$$\Delta U_{est}^+ = 0.11 \cdot \lambda_p + 0.176 \cdot \bar{k}^+ - 4.1. \quad (6)$$

In figure 3(d),  $\Delta U_{est}^+$  obtained from Eq. (6) is compared with the actual  $\Delta U^+$  from the present simulations, together with the DNS data of turbulent flow over barnacle roughness from Sarakinos & Busse (2022). Overall, good scaling can be observed. Some deviation phenomenon mainly occurs at largest and smallest  $\Delta U^+$ , which indicates that the current scaling model still has certain limitations, for instance, the area coverage cannot be too large or small. Similar scaling forms can also be extended to the ratio of the pressure drag to the total wall resistance and the normalized bulk mean velocity, as shown in figures 3(b, c). This is consistent with our previous study in three-dimensional sinusoidal rough walls (Ma *et al.*, 2020). Note that the current scaling relationships are applicable to randomly arranged or staggered rough surfaces, but the aggregation degree is not high.

Because the parameter variation of discrete rough elements is actually the parameter variation of the entire rough surface, we define a couple scale based on the overall rough surface. Then the roughness function  $\Delta U^+$  is plotted against  $\bar{k}^+ S$  in figure 4. It can be clear seen that most of the data collapse onto a single line, i.e.

$$\Delta U^+ = 1.6 \cdot \ln(\bar{k}^+ S) + 3.51. \quad (7)$$

It should be noted that Eq. (7) also has application limitations. The value of  $\bar{k}^+ S$  cannot be too large or too small. Despite these limitations, the fit embodies the basic behaviour discrete rough surfaces, which promotes the prediction of actual rough-wall resistance.

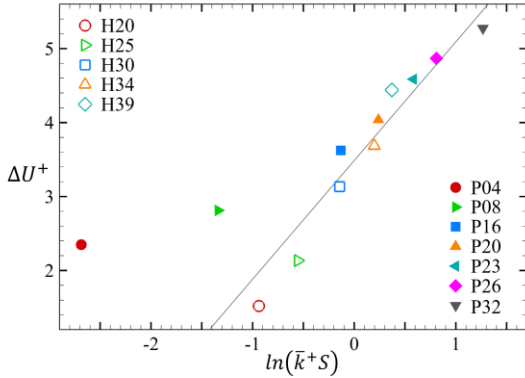


Figure 4. Plot of the roughness function versus  $\bar{k}^+ S$ .

In a rough-wall flow, variations due to the unevenness of the spatial geometry must be taken into account when analysing the turbulence statistics. Therefore, a triple decomposition is applied to the velocity where it is decomposed into three components, i.e.

$$u_i = \bar{u}_i + u'_i = U_i + \tilde{u}_i + u'_i, \quad (8)$$

where  $U_i$  denotes the time and spatial averaged component,  $\bar{u}_i$  denotes the time averaged component,  $\tilde{u}_i$  and  $u'_i$  denote the wave-induced and turbulent fluctuations, respectively.

Accordingly, the second-order velocity correlation also can be decomposed into three components, as follows:

$$\overline{u_i u_j} = \overline{(U_i + \tilde{u}_i + u'_i)(U_j + \tilde{u}_j + u'_j)} = \overline{U_i U_j} + \overline{\tilde{u}_i \tilde{u}_j} + \overline{u'_i u'_j}, \quad (9)$$

where the second and third terms on the right-hand side represent the dispersive and turbulent Reynolds stresses, respectively. The mean profiles of the streamwise turbulent Reynolds stresses and dispersive stresses are illustrated in figure 5, respectively. As shown in figures 5(a, c), the streamwise Reynolds stresses for the smooth wall reaches its maximum at  $\bar{y}^+ \approx 15$ , corresponding to the buffer layer. For the rough-wall cases, as the area coverage and the roughness height increase, the intensity of the peaks tends to decrease and they move outward away from the wall. Meanwhile, the contributions of the dispersive stresses provided in figures 5(b, d) are significant. The dispersive stresses are dominant in the vicinity of the roughness elements. Different from the turbulent Reynolds stresses, the dispersive stresses increase with the increase of the area coverage and the roughness height. It is noted that the dispersive stresses in the outer region do not decay to zero, which indicates that the current rough distribution is not completely random and has generated the weak outer large-scale flows.

## CONCLUSIONS

In the present study, DNSs were performed for turbulent channel flow over discrete rough walls. Roughness is explicitly described by body-fitted grids, and a coordinate transformation method is adopted to deal with the rough deformation. By systematically varying the area coverage or roughness height, two groups of rough-wall cases were chosen, and compared with those arising for smooth-wall turbulence at the same friction Reynolds number 540. Roughness causes a downward shift in the mean streamwise velocity profiles compared to that of the smooth-wall case, albeit still adheres to the logarithmic law distribution. The downward shift is referred to as the roughness function. The simulated cases belong to the transitionally rough regime. As the area coverage and the roughness height increase, the roughness function linearly increases. Through a simple linear fitting, the roughness function scales well with the area coverage and the roughness height, respectively. Furthermore, to better describe this scaling relationship, we introduce a couple scale  $\bar{k}^+ S$  based on the product of roughness height and steepness across the entire rough surface. A good collapse then can be observed although it still has some limitations, which is similar to the scaling properties in three-dimensional sinusoidal rough walls. For the second-order turbulence statistics, a triple decomposition method is used to extract the turbulent fluctuations from the coherent fluctuations that arise due to the rough spatial geometry. As the area coverage and the roughness height increase, the peak intensity of streamwise turbulent Reynolds stresses is notably weakened, whereas the dispersive stresses are dominant in the vicinity of the roughness elements, and increase with the increase of the area coverage and roughness height. The current scaling relationship provides an alternative rough parametrization to the equivalent sand grain roughness height  $k_s$ . For the current rough surfaces composed of discrete and randomly distributed roughness elements, more roughness parameters are still under testing, and the scaling of higher-order turbulence statistics, as well as extensions to other types of roughness, both require further investigation.

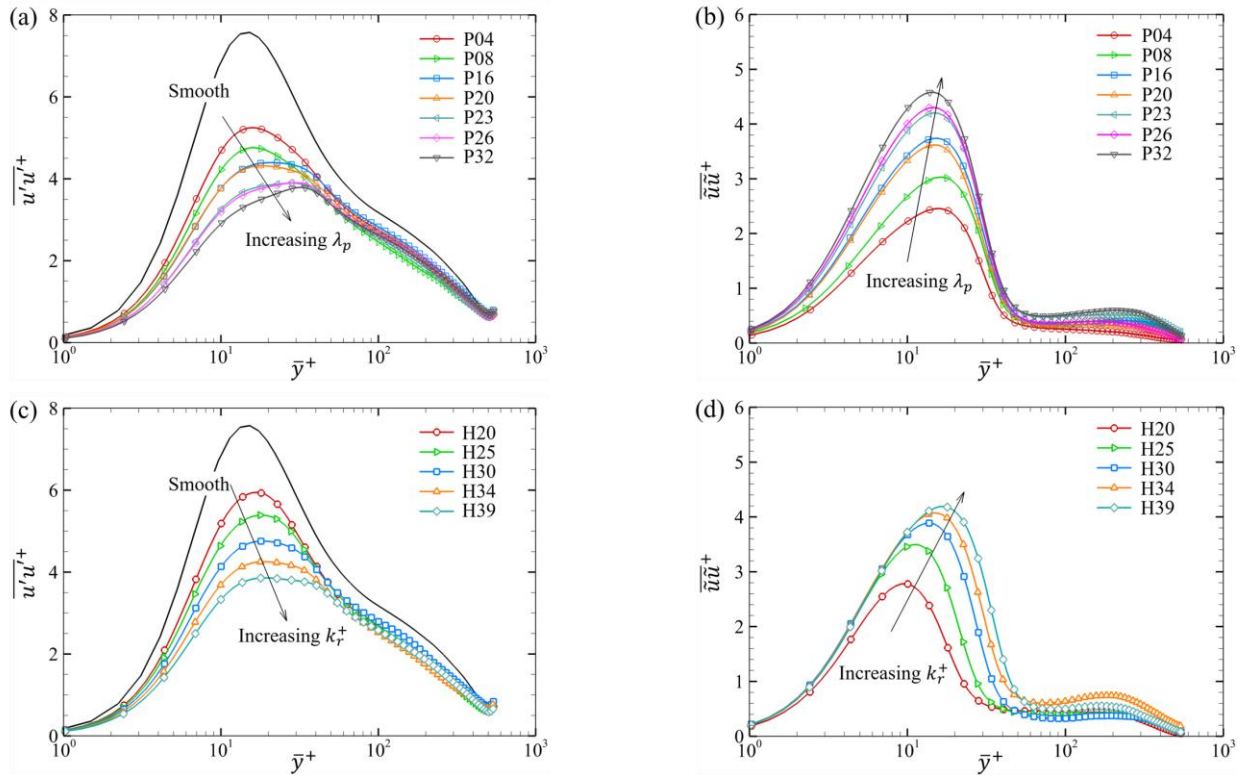


Figure 5. Profiles of (a, c) the streamwise turbulent Reynolds stresses plotted against  $\bar{y}^+$  and (b, d) the dispersive stresses plotted against  $\bar{y}^+$  for two groups of rough-wall cases, respectively.

## ACKNOWLEDGEMENTS

The authors acknowledge funding support from the National Natural Science Foundation of China under grant numbers 12272206, 92252204 and 12302289, and from the National Research Foundation of Korea under grant number 2019M3C1B7025091.

## REFERENCES

- Chung, D., Hutchins, N., Schultz, M. P., and Flack, K. A., 2021, "Predicting the drag of rough surfaces", *Annu. Rev. Fluid Mech.*, 53, 439-471.
- Ge, M. W., Xu, C. X. and Cui, G. X., 2010, "Direct numerical simulation of flow in channel with time-dependent wall geometry", *Appl. Math. Mech.*, 31 (1), 97-108.
- Ma, G. Z., Xu, C. X., Sung, H. J., and Huang, W. X., 2020, "Scaling of rough-wall turbulence by the roughness height and steepness", *J. Fluid Mech.*, 900, R7.
- Ma, G. Z., Xu, C. X., Sung, H. J., and Huang, W. X., 2023, "Secondary motions and wall-attached structures in a turbulent flow over a random rough surface", *Intl J. Heat Fluid Flow*, 102, 109147.
- MacDonald, M., Chan, L., Chung, D., Hutchins, N., and Ooi, A., 2016, "Turbulent flow over transitionally rough surfaces with varying roughness densities", *J. Fluid Mech.*, 804, 130-161.
- Nikuradse J., 1933, "Laws of flow in rough pipes", *Report No. NACA-TM-1292*.
- Sarakinos, S., and Busse A., 2022, "Investigation of rough-wall turbulence over barnacle roughness with

increasing solidity using direct numerical simulations", *Phys. Rev. Fluids*, 7(6), 064602.

Tao J. J., 2009, "Critical instability and friction scaling of fluid flows through pipes with rough inner surfaces", *Phys. Rev. Lett.*, 103, 264502.

Thakkar, M., Busse, A., and Sandham, N., 2017, "Surface correlations of hydrodynamic drag for transitionally rough engineering surfaces", *J. Turbul.*, 18(2), 138-169.